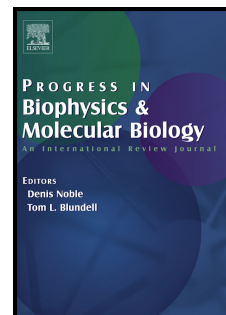


Accepted Manuscript

Title: Introducing Simulated Cellular Architecture to the Quantitative Analysis of Fluorescent Microscopy

Authors: Mark A. DePristo, Lynne Chang, Ronald D. Vale, Shahid M. Khan, Karen Lipkow



PII: S0079-6107(09)00051-0

DOI: [10.1016/j.pbiomolbio.2009.07.002](https://doi.org/10.1016/j.pbiomolbio.2009.07.002)

Reference: JPBM 587

To appear in: *Progress in Biophysics and Molecular Biology*

Please cite this article as: DePristo, M.A., Chang, L., Vale, R.D., Khan, S.M., Lipkow, K. Introducing Simulated Cellular Architecture to the Quantitative Analysis of Fluorescent Microscopy, *Progress in Biophysics and Molecular Biology* (2009), doi: 10.1016/j.pbiomolbio.2009.07.002

This is a PDF file of an unedited manuscript that has been accepted for publication. As a service to our customers we are providing this early version of the manuscript. The manuscript will undergo copyediting, typesetting, and review of the resulting proof before it is published in its final form. Please note that during the production process errors may be discovered which could affect the content, and all legal disclaimers that apply to the journal pertain.

Introducing Simulated Cellular Architecture to the Quantitative Analysis of Fluorescent Microscopy

Mark A. DePristo^{□a,b}, Lynne Chang^{□a,c}, Ronald D. Vale^{a,d},
Shahid M. Khan^{a,e,f} and Karen Lipkow^{*a,g}

^a The Physiology Course
Marine Biological Laboratory
7 MBL Street
Woods Hole, MA 02543

^b Medical and Population Genetics
Program
Broad Institute of Harvard and MIT
7 Cambridge Center
Cambridge, MA 02142

^c Department of Microbiology and
Molecular Genetics
Harvard Medical School
200 Longwood Avenue
Boston, MA 02115

^d Howard Hughes Medical Institute
Department of Cellular and Molecular
Pharmacology
University of California, San Francisco
San Francisco, CA 94107

^e Molecular Biology Consortium
Chicago Technology Park
2201 W. Campbell Park Dr.
Chicago, IL 60612

^f LUMS-School of Science &
Engineering
Lahore, Pakistan

^g Department of Biochemistry
Cambridge Systems Biology Centre
University of Cambridge
Tennis Court Road
Cambridge CB2 1QR, UK

□ These authors contributed equally to
the work.

* Corresponding author:
Email: KL280@cam.ac.uk
Phone: +44-1223-760260
Fax: +44-1223-760241

ABSTRACT

Biological cells are complex and highly dynamic: Many macromolecules are organized in loose assemblies, clusters or highly structured complexes, others exist most of the time as freely diffusing monomers. They move between regions and compartments through diffusion and enzyme-mediated transport, within a heavily crowded cytoplasm. To make sense of this complexity, computational models, and, in turn, quantitative *in vivo* data are needed. An array of fluorescent microscopy methods is available, but due to the inherent noise and complexity inside the cell, they are often hard to interpret. Using the example of fluorescence recovery after photobleaching (FRAP) and the bacterial chemotaxis system, we are here introducing detailed spatial simulations as a new approach in analysing such data.

Keywords

FRAP, Smoldyn, spatial simulation, quantification, bacterial chemotaxis

1 INTRODUCTION

1.1

Bottom-up Systems Biology takes the data produced in experimental approaches such as Molecular Biology and Genetics and builds them into computational models that simulate systems in their complexity. These aim to test whether the current concepts and thought models can work, and to find new and emergent properties in the system. Benefits of this approach include that the models are easily manipulated, allowing a test of more, and more sophisticated, variations than would be feasible experimentally, and that details can be observed which are beyond the resolution of current experimental methods.

For the simulations to be meaningful, the data they are built from have to be as good as possible. In Cellular Systems Biology, it is not only important to know which molecules react, but the rates of their binding, unbinding, and reactions; how quickly they diffuse, move or are moved; how many there are, and where they are located at which time. Most of these values are significantly different *in vitro* than in the context of a living cell. Macromolecular crowding slows down diffusion, enhances association over dissociation, and allows reactions that would be impossible in an aqueous solution (Lipkow et al., 2004; Minton, 2001). Organisation in loose assemblies, clusters or highly structured complexes enhance effectiveness (Bray et al., 1998; Sourjik and Berg, 2004). Separation onto compartments or regions keeps potentially volatile partners apart.

An array of new methods has been developed in the past few years to fulfil the need for quantitative *in vivo* data, most notably those based on fluorescent microscopy (Lippincott-Schwartz and Patterson, 2003; Phair and Misteli, 2001; Verveer and

Bastiaens, 2008). Due to the complexity of biological systems, however, their interpretation is not always straightforward. We here present a novel approach in which computational simulations are not only used to model existing data, but to extract numerical values from quantitative microscopy.

1.2

The *Escherichia coli* chemotaxis system allows the bacteria to swim to their optimum environment (**Figure 1**). It depends on two large multiprotein complexes: inputs are detected by a cluster of receptors and associated proteins at one end of the cell while laterally positioned flagellar motors generate the system's output (Kentner and Sourjik, 2006; Wadhams and Armitage, 2004). A small protein, CheY, achieves communication between these two complexes by diffusing through the cytoplasm. This protein is phosphorylated by the histidine kinase CheA, associated with the inner face of the receptor cluster, at a rate that depends on chemotactic stimulation. From there, phosphorylated CheY (CheYp) diffuses to the four-or-so motors, where it causes a change in rotational switching frequency according to its local concentration. The signal is initiated and terminated through the level of kinase activity. It adapts to constant stimulus levels and returns to its steady-state value through changes in receptor methylation by the enzymes CheR and CheB. The signal is also stopped directly through dephosphorylation of CheYp, which is promoted by the protein CheZ. CheZ, a long dimeric protein, is partially diffusing in the cytoplasm and partially bound to receptor cluster via CheA_S, a translational variant of the CheA kinase.

The bacterial chemotaxis system is arguably the best-studied signal transduction system in biology. All components are known, as well as their structures, copy numbers,

localisations, and much of the reaction kinetics (Li and Hazelbauer, 2004; Wadhams and Armitage, 2004; <http://www.pdn.cam.ac.uk/groups/comp-cell/Data.html>). This wealth of knowledge has made it a favoured subject of mathematical and computational models (Barkai and Leibler, 1997; Bray and Bourret, 1995; Bray et al., 1993; Bray et al., 2007; Mello and Tu, 2003; Shimizu et al., 2003). Most treat the bacterium as well-stirred solution. We pioneered a spatial model of the *E. coli* cell and its chemotaxis pathway using the Brownian dynamics algorithm Smoldyn (Lipkow, 2006; Lipkow et al., 2005; Lipkow and Odde, 2008), which models the movements and reactions of each relevant molecule at high spatial and temporal resolution (Andrews and Bray, 2004; <http://www.smoldyn.org/>). Building these models from published data, not much information was available on 3D protein dynamics. We therefore set out to determine the diffusion coefficients and cluster interaction dynamics of the signalling molecule and its phosphatase, CheY and CheZ.

Fluorescence recovery after photobleaching (FRAP) is a powerful method for studying the kinetic properties of a molecule including its mobility and binding interactions as well as the viscous properties of its surrounding environment (reviewed in Lippincott-Schwartz and Patterson, 2003). The method involves rapidly and irreversibly photobleaching fluorescently labelled molecules within a select region of the cell. This photobleach event effectively creates two spatially distinct populations: the photobleached molecules and unbleached, fluorescent molecules in the neighbouring regions. Mobility of the molecules can then be visualized by monitoring the recovery of fluorescence in the photobleached region by time-lapse microscopy. The fluorescence recovery resulting from the influx of unbleached molecules can be analyzed using simple

measurements to determine half-times for recovery and more complex mathematical modelling to estimate more biologically meaningful values such as the effective diffusion coefficient and the size of mobile fractions.

The analysis of FRAP data obtained on bacteria poses special challenges due to the small cell size (Elowitz et al., 1999). The low copy number of proteins results in a very noisy signal. Analysis is furthermore complicated by changing properties of molecules such as CheY and CheZ, which shuttle between a cytoplasmic and a clustered localisation. Here, we describe the use of Smoldyn simulations that deal with these problems of analysis by replicating all relevant aspects of the system. By building a cell and chemotaxis system with known parameters and varying those numbers which we were aiming to find out, we were able to deduce the missing parameters from the curves which best matched the experimental results.

2 MATERIALS AND METHODS

2.1 Bacterial Strains and Constructs

E. coli strain VS100 ($\Delta cheY$) containing plasmid pVS18 (amp^R) was obtained from Dr. H. C. Berg. pVS18 encodes CheY with a carboxy terminal fusion of EYFP separated by a three glycine linker (CheY-YFP), under control of the *pTrc* promoter (Sourjik and Berg, 2002b). Strain BC200 ($\Delta cheZ$) was obtained from Dr. M. D. Manson. Its chromosome encodes amp^R and CheZ with a carboxy terminal fusion of EGFP separated by a flexible seven amino acid linker (CheZ-GFP), under control of the *tac* promoter (Cantwell et al., 2003). VS100/pVS18 and BC200 are wildtype for chemotaxis when induced with 0.05 mM and 1 mM isopropyl- β -D-thiogalactopyranoside (IPTG) respectively (Cantwell et al., 2003; Sourjik and Berg, 2002b).

2.2 Sample Preparation

Motile cells were grown and prepared as described (Sourjik and Berg, 2004). Briefly, overnight cultures were grown while shaking in tryptone broth supplemented with 25 μ g/ml of ampicillin (TB/amp) at 30°C. Overnight cultures were diluted 1:100 into TB/amp containing IPTG (0.05 mM for VS100/pVS18 and 1 mM for BC200) and allowed to grow for 4 hr in a rotary shaker at 30°C. Slides were prepared by dispensing 100 μ l of poly-L-lysine to each well of an 8-chambered open slide. Mid-exponential cell suspensions were concentrated by centrifugation three-fold, and 100 μ l of this suspension was applied to each well, incubated for 20 min, and washed three times with 100 μ l

tethering buffer (67 mM NaCl, 10 mM potassium phosphate (pH 7), 100 μ M EDTA, 1 μ M L-methionine, 10 mM sodium lactate (pH 7.0) (Khan et al., 2004)).

2.3 FRAP Microscopy and Analysis

Cell populations were screened for the presence of polar clusters on a Zeiss Axioplan microscope with a Plan Apochromat 40x 1.0 NA oil immersion objective at room temperature ($\sim 22^{\circ}\text{C}$). Cells exhibited a pronounced cluster of fluorescence at one or both poles or were uniformly fluorescent.

Confocal microscopy and FRAP were performed at room temperature ($\sim 22^{\circ}\text{C}$) on an LSM 510 confocal microscope (Carl Zeiss, Inc., Thornwood, NY) with a Plan Apochromat 100x 1.4 NA oil immersion objective and an Argon ion laser (30 mW power, 6.5 A tube current).

For FRAP, individual cells were selected from phase-contrast and fluorescence images, and the scan region was limited to include only the subject and one or two other cells. For cells with clusters, the bleach zone was selected to include only the pole. For FRAP of cytosolic molecules, the zone was positioned over an arbitrary end of a diffuse cell so as to include approximately one third of the cell body. For each cell, three pre-bleach fluorescence images were captured followed by photo-bleaching at 488 nm for CheZ-GFP and 514nm for CheY-YFP (100% laser power; average photobleach duration = 186 ms, standard deviation = 87 ms). Recovery of fluorescence was monitored (3% laser power) using the time-series function with no cycle delay and frame scan rates ranging from 41-319 ms. Parallel measurements were taken from a region of similar size in a neighbouring unbleached cell. The integrated intensities of the bleached (I_{bleached}) and

unbleached ($I_{\text{unbleached}}$) regions for the FRAP experiments were calculated using the Zeiss LSM 510 analysis software. Frames were normalized so that the bleach event occurred at time $t = 0.0$ s. To account for the photobleaching we expressed the recovery as a ratio of (I_{bleached}) / ($I_{\text{unbleached}}$).

2.4 Smoldyn Simulations

Simulations were performed with version 1.58 of the Brownian Dynamics simulator Smoldyn (Andrews and Bray, 2004); <http://www.smoldyn.org/>. The simulations were set up by modelling a single bacterium as a rectangular box of $1.2 \mu\text{m} \times 0.88 \mu\text{m} \times 0.88 \mu\text{m}$, having the same volume and proportion as an average *E. coli* cell. For FRAP experiments on cells lacking polar clusters, the cell volume was partitioned into a “bleached zone” occupying 1/3 of the cell with the remainder being the “unbleached zone”. The cell was populated with randomly positioned protein molecules, based on published estimates: We chose 16,000 CheY-YFP monomers, as measured for our induction conditions (Sourjik and Berg, 2002a), and 1,600 CheZ dimers, as measured in wildtype cells in rich medium (Li and Hazelbauer, 2004). For modelling FRAP experiments on cells with polar clusters, the bleached volume was taken to be approximately diffraction limited ($0.3 \mu\text{m} \times 0.88 \mu\text{m} \times 0.88 \mu\text{m}$). The bleached zones in both cases mimicked the standards used in the experiments. The cluster was modelled as a $0.72 \mu\text{m} \times 0.72 \mu\text{m}$ patch adjacent to the membrane in the bleached zone. We worked with the assumption that there are 3000 and 1000 available binding sites for CheY and CheZ respectively, derived from the molecule numbers measured in wt cells, 4500 CheA_L and 2200 CheA_S monomers (Li and Hazelbauer, 2004). CheY binds to the CheA P2 domain (Swanson et al., 1993), which is present in both translational variants; one or

two CheY molecules each will therefore be able to bind to most of the 3350 dimers of any composition. CheZ binds selectively to the truncated P1 domain of CheA_S (Cantwell et al., 2003; Wang and Matsumura, 1996); assuming unbiased dimerisation efficiency, CheZ will therefore have on average 391 A_SA_S and possibly up to 1478 A_LA_S binding targets. No attempt was made to distinguish between CheY and CheYp.

Changing cytoplasmic positions of the free CheY and CheZ molecules and their patch occupancies were simulated at time steps of 0.1 ms. Local concentration effects were simulated by changing patch size. The molecules were colour-coded. After a time delay, to allow the pre-bleach steady state to be attained, “bleaching” was effected by changing the colour-code of the cytoplasmic molecule. As diffusion and unimolecular reactions, the bleaching reaction was stochastic: Each molecule in the relevant zone was converted with a probability of P (e.g. P = 0.315 for **Figure 5B**). Lists of the molecule positions with time, read out at 0.2 s intervals, were processed using MATLAB version 7.0 (Mathworks Inc. Natick, MA) to generate FRAP recovery trajectories for comparison with the experimental data. For **Figure 5** and Supplementary movies 3 and 4, TIFFs of the simulation were generated from within Smoldyn, and the background colour changed with Adobe Photoshop CS2.

3 RESULTS

3.1 Localization of Fluorescent Protein Fusions

Immobilized cells of *E. coli* strains VS100/pVS18, expressing CheY-YFP, and BC200, expressing CheZ-GFP, exhibited pronounced localization of their fluorescence, in accordance with previous studies (Cantwell et al., 2003; Sourjik and Berg, 2000). While we did not attempt to subdivide the observed clusters into polar clusters versus the more diffuse patches (Skidmore et al., 2000; Sourjik and Berg, 2000), our impression was that the large majority of the clusters were tight rather than diffuse. The distribution of the clusters in the cell population was heterogeneous in both cases. Within one population, bacteria with uniform, mono-polar or bi-polar clustered fusion protein distributions were all found. Cell-to-cell variation in expression level may account, in part, for this heterogeneity.

The population fraction for the three distribution types for CheZ-GFP was found to depend on the level of induction. At a physiological expression level, i.e. the IPTG concentration needed to obtain wildtype chemotactic behaviour (1mM), c. 90% of the cells had at least one clear cluster (**Figure 2**). At reducing the inducer concentration, only c. 25% of cells displayed any clustering, but at increasing it 10 fold, no significant change was observed. This implies that the distribution obtained at physiological levels was close to saturation and that the lack of clusters in a proportion of the cells has to be due to other reasons than expression levels, such as dynamic protein localisation of CheZ in response to signalling state (Lipkow, 2006). IPTG levels needed to obtain physiological levels of the fusion proteins were used for the FRAP studies.

3.2 Determination of Diffusion Coefficients

To measure cytoplasmic dynamics for the two proteins independently from their association with the polar cluster, we chose cells lacking polar clusters from the experimental population. We laser photo-bleached part (ca. 1/3) of the cells (**Figure 3A**). Ten or more cells were bleached for each of the CheY-YFP and CheZ-GFP cell populations. From each set, 5-6 example traces are shown in **Figure 4A** and **B**. The recovery trajectories are very noisy, and only those for CheY-YFP were suitable to be fitted by single exponentials ($I - Ae^{-Bt}$) as expected (Elowitz et al., 1999). The decrease in fluorescence intensity of CheZ-GFP in response to photo-bleaching was less relative to the decrease observed with CheY-YFP, consistent with the three-fold higher photostability of EGFP versus EYFP (Shaner et al., 2007).

The FRAP recovery data in cells lacking clusters were modelled based on the assumption that the molecules were homogenous (had a single diffusion coefficient) in an isotropic environment. We created *in silico* cells of the volume and proportions of *E. coli* cells and populated them randomly with our best estimation of CheY-YFP or CheZ-GFP molecule numbers (16,000 and 1,600 respectively, see Materials and Methods). As above, we simulated the photobleaching event by simultaneously converting a fraction of the molecules in one third of the cell to a differently coloured species (**Figure 5A**). Both the volume and the fraction of molecules bleached was based on our FRAP experiments. Coloured and bleached molecules were allowed to continue diffusing with the same diffusion coefficient, and their distribution throughout the cell was recorded.

Simulated recovery curves show the same level of noise as the experiments (**Figure 6**). We ran the simulations with a series of diffusion coefficients, in five

repetitions each. For CheY-YFP, these could be fitted by single exponentials. Both the exponential fits and the shape of the recovery traces were closest to the experimental measurements at a diffusion coefficient of $2 \mu\text{m}^2\text{s}^{-1}$ (**Figure 6A,B**, compare with **Figure 4A**).

Due to the 10x lower molecule numbers, the CheZ-GFP curves are a lot noisier. The mean standard deviation for the CheZ-GFP traces is about 5%, while that for the CheY-YFP traces should be $(10)^{0.5} = 3.3$ times smaller, consistent with our observations. The best match between simulated and experimentally measured curves was achieved with a diffusion coefficient of $2 \mu\text{m}^2\text{s}^{-1}$ (**Figure 6C**, compare with **Figure 4B**).

3.3 Determination of Binding Coefficients

Ten cells in each strain with a polar cluster were chosen for FRAP study of the interaction dynamics of the proteins with the cluster. The cluster was more prominent in CheZ-GFP containing cells due to a lower cytosolic background, compared to cells expressing CheY-YFP when the proteins were expressed at physiological concentrations. When a cytosolic region was photo-bleached in CheY-YFP localized cells, the entire cell's fluorescence rapidly diminished, implying that the clustered CheY-YFP exchanged rapidly with the cytosolic pool. Most FRAP-curves of clustered CheY-YFP exhibited near-complete recovery, but at a slower rate than the cytosolic CheY-YFP in diffuse cells (**Figure 4C**).

Polarly localized CheZ-GFP exhibited a radically different behaviour than diffuse CheZ-GFP or polarly-localized CheY-YFP (**Figure 4D**). The laser photo-bleaching pulse created a dark pole that lasted for at least 20 s without appreciable recovery (**Figure 3B**). An initial, slight recovery was presumably due to exchange of CheZ-GFP

molecules between the bleached and unbleached cytoplasmic zones. Observations of the photo-bleached cells beyond 20 s were difficult due to gradual bleaching of the entire cell fluorescence by the monitoring laser beam. In the reverse experiment (photo-bleaching of a central cytosolic region), the polar patch was left as a bright spot against a dark intracellular background over tens of seconds (data not shown). The fact that under the same experimental conditions, cells containing CheY-YFP or uniformly distributed CheZ-GFP completely recovered their fluorescence profiles ruled out cell damage as responsible for the lack of recovery seen in cells with polarly localized CheZ-GFP.

The cluster was modelled as a polar patch as detailed in Materials and Methods (**Figure 5B**). We examined the effect on FRAP kinetics of local binding site concentration by changing patch size from $1.3 \mu\text{m}^2/\text{receptor}$ to $10^3 \text{ nm}^2/\text{receptor}$. There was a modest effect (ca. 25%) on steady state patch occupancies, but not on FRAP kinetics. Thus, local concentrations effects are not significant over this range of receptor densities.

Next, we estimated the affinities needed to make clusters visible over the cytoplasmic background. Brownian dynamics simulations by Northrup and Erickson (1992) revealed that due to the stereo-specificity of such interactions, the typical diffusion-limited on rate (k_{on}) for protein-protein associations is ca. $(2-6) \times 10^6 \text{ M}^{-1}\text{s}^{-1}$. This was fixed at $6 \times 10^6 \text{ M}^{-1}\text{s}^{-1}$ and the dissociation constant, K_{D} , changed by changing k_{off} . We found that visible clusters will only be observed if the K_{D} for CheY and CheZ is $< 10 \mu\text{M}$ ($k_{\text{off}} < 10^2 \text{ s}^{-1}$). At saturation, a CheZ-GFP cluster will be much brighter than the CheY-YFP cluster relative to the cytosolic background; due to the fact that the pool

of cytosolic CheZ is much smaller than that for CheY while saturation patch occupancies are similar (**Figure 7A**).

Comparing the simulated recovery curves with the experimentally obtained ones revealed a good match for the following values: CheY-YFP: $k_{\text{off}} = 1 \text{ s}^{-1}$, giving a K_D in the order of $0.1 \text{ }\mu\text{M}$ (**Figure 7B**, compare with **Figure 4C**). CheZ-GFP: $k_{\text{off}} = 0.01 \text{ s}^{-1}$, giving a K_D in the order of 1 nM (**Figure 7C**, compare with **Figure 4D**). With these values, and the diffusion coefficient of $2 \text{ }\mu\text{m}^2\text{s}^{-1}$, the measured and simulated curves are similar in overall shape, recovery level, recovery time and noise level.

4 DISCUSSION

4.1

Our strategy shows the application of simulations as a powerful new technique to extract quantitative information from complex experimental data. Demonstrating the detail of our method, the level of noise we observed was comparable in experiments and simulations. This confirms the published numbers (Cantwell et al., 2003; Li and Hazelbauer, 2004; Sourjik and Berg, 2002a) and means also that the noise was due to the low number of molecules and inherent stochasticity, and not due to potential limitations of the equipment.

Conducted within the time-constraints of a summer course, we only managed a limited number of repetitions and used unconfirmed estimates for some of the numbers that went into our model. Nevertheless, our results are within the same order of magnitude as a more thorough study that was carried out in the meantime (Schulmeister et al., 2008), and our diffusion coefficient for CheY-YFP is even within the margin of error of their best estimate. They also chose to use numerical methods to quantify their complex FRAP data.

Our estimated apparent diffusion coefficient for CheY-YFP is lower than that determined for GFP-CheY ($4.6 \mu\text{m}^2\text{s}^{-1}$) in *Salmonella typhimurium* (Cluzel et al., 2000) and than the normally assumed value of $10 \mu\text{m}^2\text{s}^{-1}$ (Sourjik and Berg, 2002a). The difference between the experimentally determined and calculated values could be due to a number of factors such as concentration effects (Elowitz et al., 1999), macromolecular crowding (Hall and Minton, 2003) and interactions with other cytoplasmic proteins,

including CheY binding partners CheA, CheZ and FliM. In line with its role as a diffusible messenger molecule, CheY-YFP was found to have a lower affinity to the receptor cluster than CheZ-GFP. It is important to point out that we have investigated the behaviour of CheY-EYFP and CheZ-EGFP, not of CheY and CheZ on their own. At a molecular weight of c. 28 kDa, GFP and its variants are heavier than both CheY (14 kDa) and CheZ (24 kDa), and might well dominate the diffusion properties of the fusion proteins.

FRAP of cytosolic and clustered proteins is not the only technique that can be enhanced by Smoldyn simulations. We already used it to quantify the clearance of antibody-labelled membrane proteins in auditory hair cells (Grati et al., 2006). Other suitable kinetic microscopy techniques include photoactivation or photoconversion, FRET (Förster resonance energy transfer), FLIP (fluorescence loss in photobleaching), and FCS (fluorescence correlation spectroscopy). Photoactivation and photoconversion are alternate methods to photobleaching for visualizing a subpopulation of molecules by selectively initiating or altering fluorescence emission profiles (Lukyanov et al., 2005). FRET is a distance-dependent transfer of energy between an excited donor molecule and an acceptor molecule and a widely used technique for determining protein-protein interactions as well as conformational changes within a protein (Piston and Kremers, 2007). In FLIP, a small region of the cell is repeatedly photobleached while the loss in fluorescence in the surrounding area is monitored to analyze the mobility of the fluorescently tagged molecule (Lippincott-Schwartz et al., 2001). In FCS, a small, defined volume in the femtoliter range is monitored for fluctuations in the fluorescence signal, over a short period of time (Van Craenenbroeck and Engelborghs, 2000). These

fluctuations can be analyzed to determine the concentration of the proteins in the sample volume as well as diffusion coefficients and binding constants.

Smoldyn employs the Smoluchowski level of detail, generally representing molecules as individual points in continuous space. Development is ongoing; its current version (2.03) can model internal surfaces and molecules with excluded volume. This allows simulation of very complex cellular structures, including eukaryotic cells with their membrane-bound compartments. Great care has been employed in its development, and at the level relevant for cell biology, it is exceptionally accurate. This makes it an excellent analysis tool: The user can trust the results to be biophysically correct, and does not need to develop the equations on his own every time.

4.2 Conclusion

Fluorescent microscopy has contributed tremendously toward our understanding of the inner workings of a cell and brought to light much of the inherent intricate structural complexity. It is this aspect that now makes accurate quantification of microscopy data hard to do by conventional methods. We show a first instance of how to add back some of that structural complexity into the analysis process.

ACKNOWLEDGEMENTS

This project was carried out as part of the 2004 Physiology course at the Marine Biological Laboratory (MBL). We thank the course instructors and students, particularly Drs. Tim Mitchison and Dennis Bray, for discussions, and Dr Steven Andrews for assistance with Smoldyn. We are indebted to MBL and Rudi Rottenfusser (Carl Zeiss, Inc.) for loan and help with the microscopy equipment and thank Sven Sewitz for valuable suggestions on the manuscript. We received additional support from MBL post-course research fellowships (MAD and LC), the Bauer Center for Genomic Research, a National Science Foundation graduate research fellowship (MAD), a MERIT Award (LC), grants RO1-GM64713 (Dennis Bray) and RO1-GM49319 (SMK) from the National Institutes of Health, and a Royal Society University Research Fellowship (KL). We wish Dennis Bray many happy returns.

REFERENCES

- Andrews, S. S. and Bray, D. (2004) Stochastic simulation of chemical reactions with spatial resolution and single molecule detail. *Phys Biol* **1**, 137-51.
- Barkai, N. and Leibler, S. (1997) Robustness in simple biochemical networks. *Nature* **387**, 913-7.
- Bray, D. and Bourret, R. B. (1995) Computer analysis of the binding reactions leading to a transmembrane receptor-linked multiprotein complex involved in bacterial chemotaxis. *Mol Biol Cell* **6**, 1367-80.
- Bray, D., Bourret, R. B. and Simon, M. I. (1993) Computer simulation of the phosphorylation cascade controlling bacterial chemotaxis. *Mol Biol Cell* **4**, 469-82.
- Bray, D., Levin, M. D. and Lipkow, K. (2007) The chemotactic behavior of computer-based surrogate bacteria. *Curr Biol* **17**, 12-9.
- Bray, D., Levin, M. D. and Morton-Firth, C. J. (1998) Receptor clustering as a cellular mechanism to control sensitivity. *Nature* **393**, 85-8.
- Cantwell, B. J., Draheim, R. R., Weart, R. B., Nguyen, C., Stewart, R. C. and Manson, M. D. (2003) CheZ phosphatase localizes to chemoreceptor patches via CheA-short. *J Bacteriol* **185**, 2354-61.
- Cluzel, P., Surette, M. and Leibler, S. (2000) An ultrasensitive bacterial motor revealed by monitoring signaling proteins in single cells. *Science* **287**, 1652-5.
- Elowitz, M. B., Surrrette, M. G., Wolf, P.-E., Stock, J. B. and Leibler, S. (1999) Protein mobility in the cytoplasm of *Escherichia coli*. *J Bacteriol* **181**, 197-203.
- Grati, M., Schneider, M. E., Lipkow, K., Strehler, E. E., Wenthold, R. J. and Kachar, B. (2006) Rapid turnover of stereocilia membrane proteins: evidence from the trafficking and mobility of plasma membrane Ca(2+)-ATPase 2. *J Neurosci* **26**, 6386-95.
- Hall, D. and Minton, A. P. (2003) Macromolecular crowding: qualitative and semiquantitative successes, quantitative challenges. *Biochim Biophys Acta* **1649**, 127-39.
- Kentner, D. and Sourjik, V. (2006) Spatial organization of the bacterial chemotaxis system. *Curr Opin Microbiol* **9**, 619-24.
- Khan, S., Jain, S., Reid, G. P. and Trentham, D. R. (2004) The fast tumble signal in bacterial chemotaxis. *Biophys J* **86**, 4049-58.
- Li, M. and Hazelbauer, G. L. (2004) Cellular stoichiometry of the components of the chemotaxis signaling complex. *J Bacteriol* **186**, 3687-94.
- Lipkow, K. (2006) Changing cellular location of CheZ predicted by molecular simulations. *PLoS Comput Biol* **2**, e39. DOI: 10.1371/journal.pcbi.0020039.eor.

- Lipkow, K., Andrews, S. S. and Bray, D. (2005) Simulated diffusion of phosphorylated CheY through the cytoplasm of *Escherichia coli*. *J Bacteriol* **187**, 45-53.
- Lipkow, K., Buisine, N. and Chalmers, R. (2004) Promiscuous target interactions in the mariner transposon Himar1. *J Biol Chem* **279**, 48569-75.
- Lipkow, K. and Odde, D. J. (2008) Model for Protein Concentration Gradients in the Cytoplasm. *Cellular and Molecular Bioengineering* **1**, in press.
- Lippincott-Schwartz, J. and Patterson, G. H. (2003) Development and use of fluorescent protein markers in living cells. *Science* **300**, 87-91.
- Lippincott-Schwartz, J., Snapp, E. and Kenworthy, A. (2001) Studying protein dynamics in living cells. *Nat Rev Mol Cell Biol* **2**, 444-56.
- Lukyanov, K. A., Chudakov, D. M., Lukyanov, S. and Verkhusha, V. V. (2005) Innovation: Photoactivatable fluorescent proteins. *Nat Rev Mol Cell Biol* **6**, 885-91.
- Mello, B. A. and Tu, Y. (2003) Perfect and near-perfect adaptation in a model of bacterial chemotaxis. *Biophys J* **84**, 2943-56.
- Minton, A. P. (2001) The influence of macromolecular crowding and macromolecular confinement on biochemical reactions in physiological media. *J Biol Chem* **276**, 10577-80.
- Northrup, S. H. and Erickson, H. P. (1992) Kinetics of protein-protein association explained by Brownian dynamics computer simulation. *Proc Natl Acad Sci U S A* **89**, 3338-42.
- Phair, R. D. and Misteli, T. (2001) Kinetic modelling approaches to in vivo imaging. *Nat Rev Mol Cell Biol* **2**, 898-907.
- Piston, D. W. and Kremers, G. J. (2007) Fluorescent protein FRET: the good, the bad and the ugly. *Trends Biochem Sci* **32**, 407-14.
- Schulmeister, S., Ruttorf, M., Thiem, S., Kentner, D., Lebiedz, D. and Sourjik, V. (2008) Protein exchange dynamics at chemoreceptor clusters in *Escherichia coli*. *Proc Natl Acad Sci U S A* **105**, 6403-8.
- Shaner, N. C., Patterson, G. H. and Davidson, M. W. (2007) Advances in fluorescent protein technology. *J Cell Sci* **120**, 4247-60.
- Shimizu, T. S., Aksenov, S. V. and Bray, D. (2003) A spatially extended stochastic model of the bacterial chemotaxis signalling pathway. *J Mol Biol* **329**, 291-309.
- Skidmore, J. M., Ellefson, D. D., McNamara, B. P., Couto, M. M., Wolfe, A. J. and Maddock, J. R. (2000) Polar clustering of the chemoreceptor complex in *Escherichia coli* occurs in the absence of complete CheA function. *J Bacteriol* **182**, 967-73.
- Sourjik, V. and Berg, H. C. (2000) Localization of components of the chemotaxis machinery of *Escherichia coli* using fluorescent protein fusions. *Mol Microbiol* **37**, 740-51.

- Sourjik, V. and Berg, H. C. (2002a) Binding of the *Escherichia coli* response regulator CheY to its target measured *in vivo* by fluorescence resonance energy transfer. *Proc Natl Acad Sci U S A* **99**, 12669-74.
- Sourjik, V. and Berg, H. C. (2002b) Receptor sensitivity in bacterial chemotaxis. *Proc Natl Acad Sci U S A* **99**, 123-7.
- Sourjik, V. and Berg, H. C. (2004) Functional interactions between receptors in bacterial chemotaxis. *Nature* **428**, 437-41.
- Swanson, R. V., Schuster, S. C. and Simon, M. I. (1993) Expression of CheA fragments which define domains encoding kinase, phosphotransfer, and CheY binding activities. *Biochemistry* **32**, 7623-9.
- Van Craenenbroeck, E. and Engelborghs, Y. (2000) Fluorescence correlation spectroscopy: molecular recognition at the single molecule level. *J Mol Recognit* **13**, 93-100.
- Verveer, P. J. and Bastiaens, P. I. (2008) Quantitative microscopy and systems biology: seeing the whole picture. *Histochem Cell Biol* **130**, 833-43.
- Wadhams, G. H. and Armitage, J. P. (2004) Making sense of it all: bacterial chemotaxis. *Nat Rev Mol Cell Biol* **5**, 1024-37.
- Wang, H. and Matsumura, P. (1996) Characterization of the CheAS/CheZ complex: a specific interaction resulting in enhanced dephosphorylating activity on CheY-phosphate. *Mol Microbiol* **19**, 695-703.

Figure Legends

Figure 1: Schematic of the chemotactic signalling pathway in *Escherichia coli*. Dimeric proteins are indicated by double letters. Colours as in **Figure 3** and **Figure 5**.

Figure 2: Fraction of uniform, mono-polarly and bi-polarly fluorescent CheZ-GFP expressing cells as a function of IPTG inducer concentration. $1x = 1 \text{ mM}$, the concentration required to obtain wild-type phenotype (Cantwell et al., 2003). Over 200 cells were examined for each induction condition.

Figure 3: Representative FRAP time series for diffuse CheY-YFP (A) and localized CheZ-GFP (B). The first image in each series shows unbleached cells with the subsequent bleach zone encircled in red. Following frames show selected images from the entire FRAP series, annotated with its time relative to the bleach event ($t = 0.0$) in seconds.

Figure 4: Individual FRAP experiment traces for diffuse CheY-YFP (A), diffuse CheZ-GFP (B), clustered CheY-YFP (C), and clustered CheZ-GFP (D). The bleach event occurs at 0 seconds in all cases. Continuous lines denote single exponential fits ($I - Ae^{-Bt}$) to the data, colour coded to match the data points ($B = 2.8 \pm 0.8$; $n = 6$).

Figure 5: Graphical output from Smoldyn simulations. The subsequent bleach zone is marked in red. (A) Diffuse CheY-YFP, as in **Figure 3A**. CheY-YFP molecules (yellow) are distributed randomly in the cell. At $t=0.0$, c. 31.5% of fluorescent molecules in the bleach zone are replaced by bleached molecules (grey). (B) Clustered CheZ-GFP, as in **Figure 2B**. The binding sites (CheA_s, red) are randomly positioned and immobilized

within the square patch at the bottom. After 2-5 s to allow saturated binding of CheZ-GFP (green) to CheA_S, c. 55% of both free and clustered fluorescent molecules were bleached in the marked zone by replacing them with dark green ones.

Figure 6: Simulated FRAP recovery curves for uniformly fluorescent cell populations. (A) CheY-YFP; $D = 2, 1$ and $0.5 \mu\text{m}^2\text{s}^{-1}$. Solid lines: best single exponential fits (see text). (B) Five stochastically simulated CheY-YFP recovery trajectories for $D = 2 \mu\text{m}^2\text{s}^{-1}$. (C) Five stochastically simulated CheZ-GFP recovery trajectories for $D = 2 \mu\text{m}^2\text{s}^{-1}$.

Figure 7: Simulated binding and FRAP recovery for cells with clustered fusion proteins. (A) Relative cluster intensity (fluorescence ratio of the polar, diffraction-limited zone containing the receptor patch over an equivalent, cytosolic volume) as a function of k_{off} . 16,000 CheY-YFP monomers (black bars); 1,600 CheZ-GFP dimers (grey bars). $D = 2 \mu\text{m}^2\text{s}^{-1}$, $k_{\text{on}} = 6 \times 10^6 \text{ M}^{-1}\text{s}^{-1}$. A visible cluster will only be obtained if the ratio is > 1 . (B & C) Simulated FRAP recovery curves; D and k_{on} as in A. (B) CheY-YFP and (C) CheZ-GFP expressing cells with polar clusters. No binding (—■—), $k_{\text{off}} = 10^3$ (—■—), 10^2 (—■—), 10 (—■—), 1 (—■—), 0.1 (—■—), 0.01 (—■—) and 0.001 (—■—) s^{-1} .

Supplementary Material

Supplementary Movie 1. FRAP of time series for CheY diffuse (as **Figure 3A**).

Supplementary Movie 2. FRAP of time series for CheZ clustered (as **Figure 3B**).

Supplementary Movie 3. Simulated time series for CheY diffuse (as **Figure 5A**), in real time. At $t = 2$ s, the rightmost third of the cell is partially bleached by replacing 31.5% of yellow CheY-YFP with grey bleached molecules.

Supplementary Movie 4. Simulated time series for CheZ clustered (as **Figure 5B**), in real time. The receptor / CheA cluster is located at the right pole. At $t = 2$ s, a slice of 300 nm width including the cluster is partially bleached by replacing 55% of bright green CheZ-GFP with dark green bleached molecules.

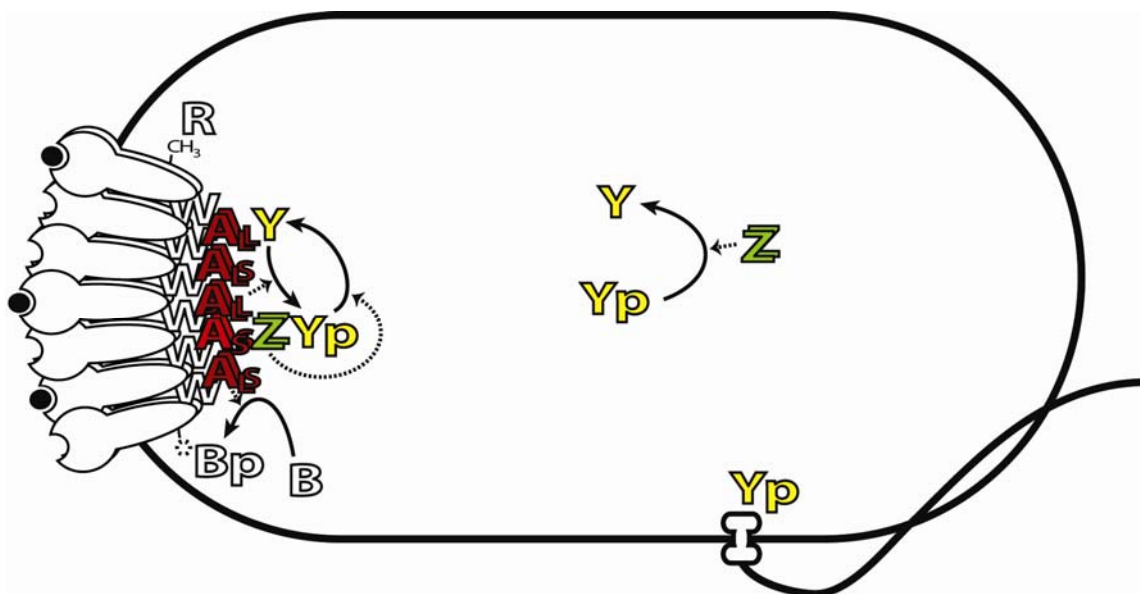


Figure 1

ACCI

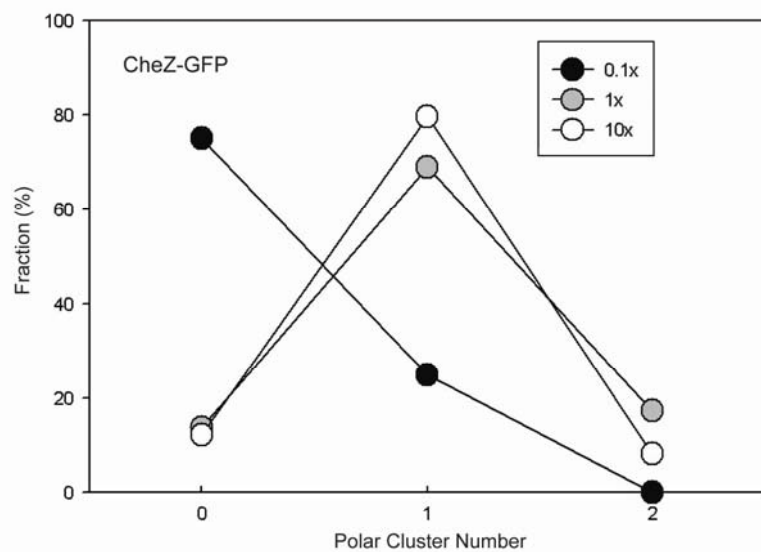


Figure 2

ACCEPT

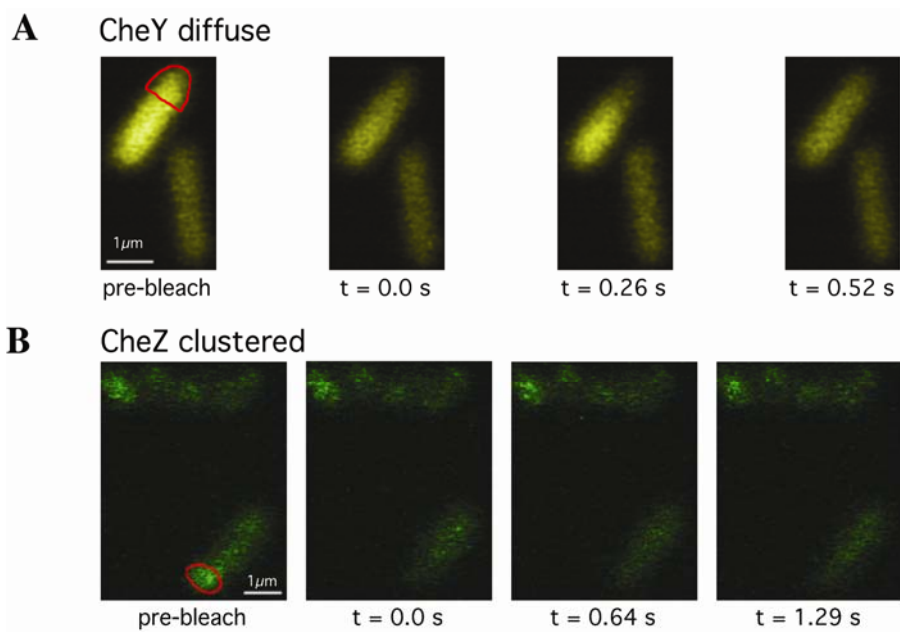


Figure 3

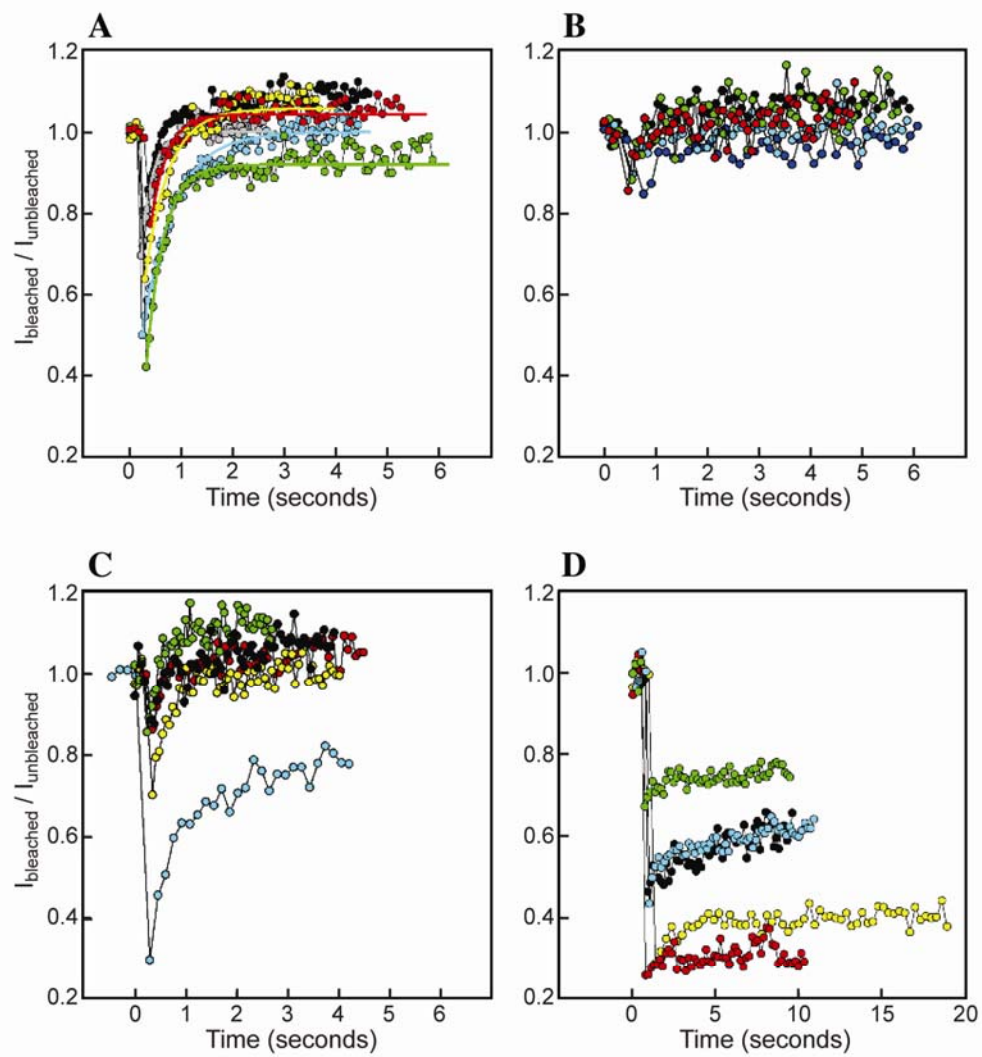


Figure 4

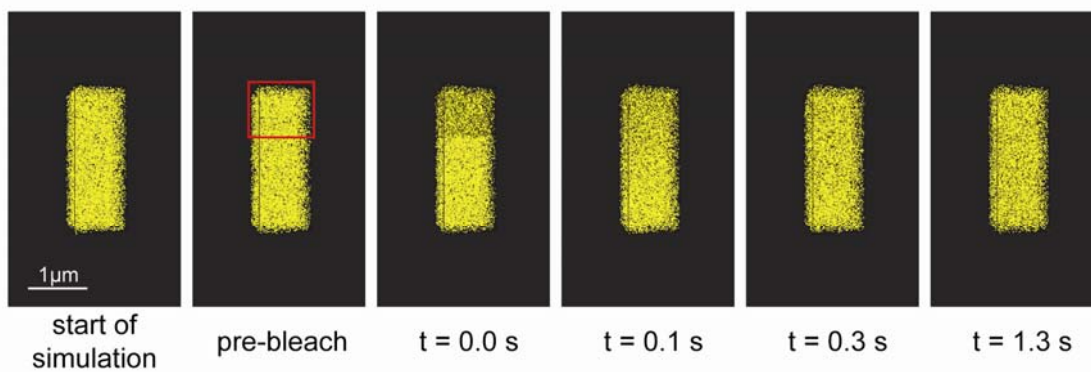
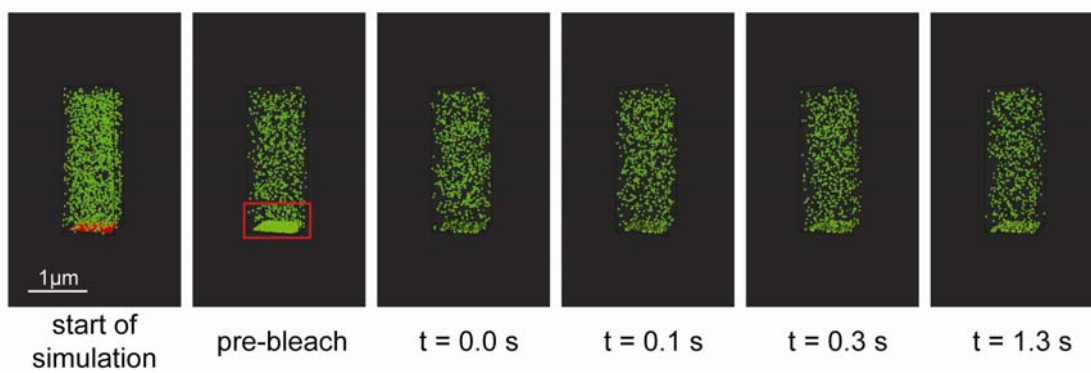
A CheY diffuse**B** CheZ clustered

Figure 5

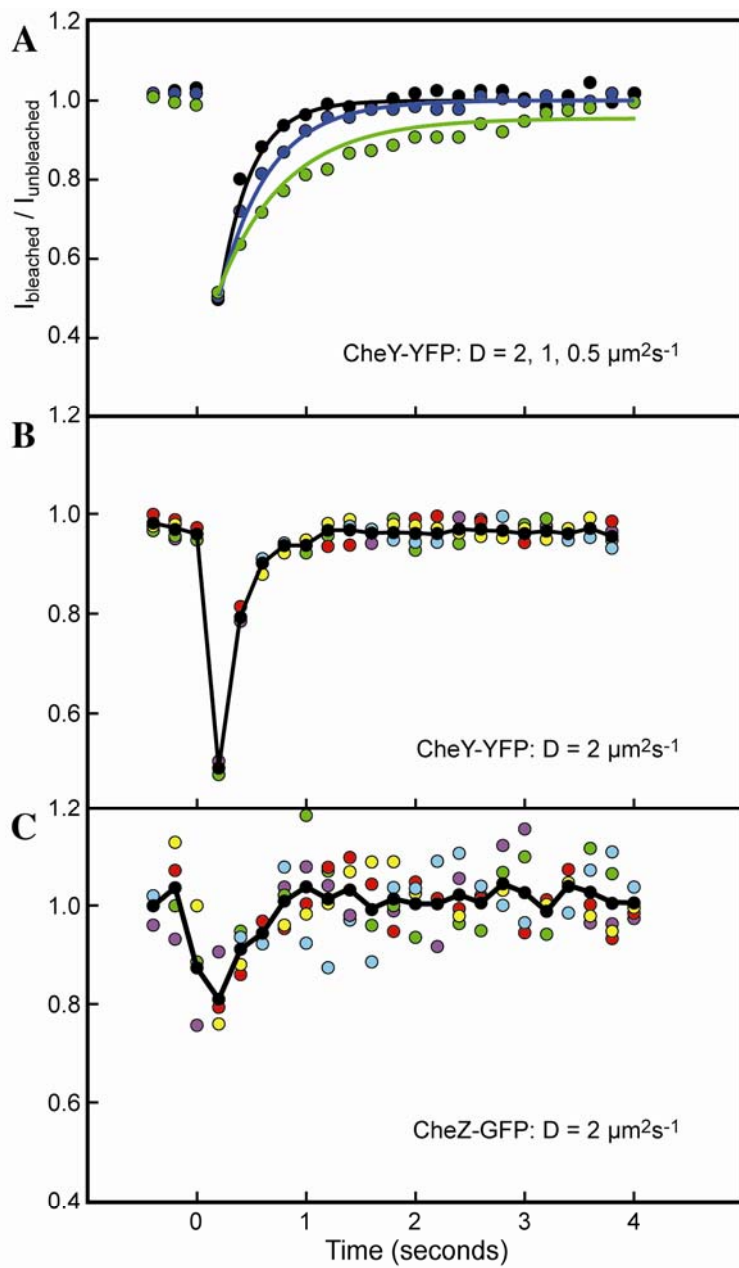


Figure 6

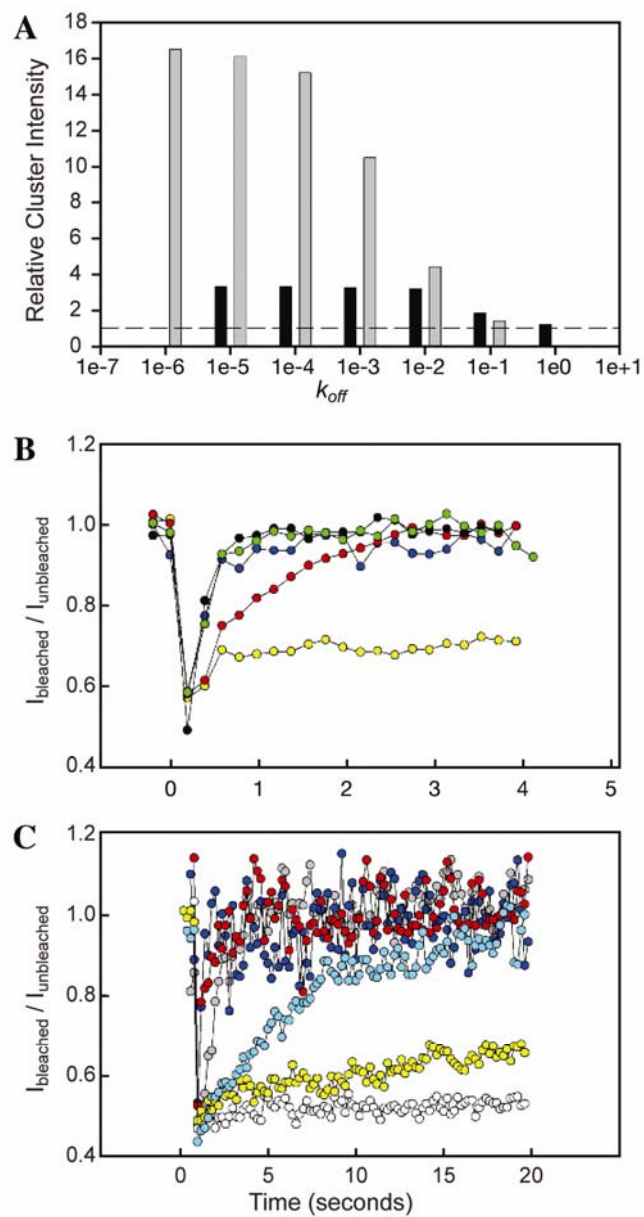


Figure 7